

# Platinum Activity for CO Electrooxidation: from Single Crystal Surfaces to Nanosurfaces and Real Fuel Cell Nanoparticles

Christophe Coutanceau · Claude Lamy ·  
Patrick Urchaga · Stève Baranton

Published online: 30 March 2012  
© Springer Science+Business Media, LLC 2012

**Abstract** The understanding of CO oxidation on platinum catalysts is a key point in several low-temperature fuel cell technologies: direct-alcohol fuel cells or proton-exchange membrane fuel cell fed with reformat hydrogen, for example. For this purpose, studies were carried out on different platinum surfaces, from single crystals surfaces with a well-defined orientation to platinum nanoparticle polyoriented surfaces. This article presents the CO electrooxidation on surfaces of Pt single crystals and Pt nanoparticles with different orientations and size ranges. The study of CO oxidation was completed with in situ reflectance spectroscopy coupled to electrochemical methods. The confrontation of CO oxidation behaviours observed on electrodes with oriented surfaces at macroscopic and nanoscopic size ranges allowed establishing a correlation between the surface structure and the CO oxidation voltammetric features.

**Keywords** CO oxidation · Platinum · Single crystals · Shaped nanoparticles · In situ FTIRS

## Introduction

In many electrochemical reactions occurring in low-temperature fuel cells with Pt-based anodes, CO is a key molecule, since it is always present in different amounts

---

This paper is dedicated to our close friend Radoslav Adžič for his 70th birthday.

---

C. Coutanceau (✉) · C. Lamy · P. Urchaga · S. Baranton  
GDR CNRS 3339 (PACS),  
Unniversité de Poitiers, IC2MP, UMR CNRS 7285,  
4 rue Michel Brunet, B 27,  
86022 Poitiers, France  
e-mail: Christophe.coutanceau@univ-poitiers.fr

(depending on the clean-up process) in a reformat gas obtained, e.g. by methane steam reforming. A few ppm of CO in the hydrogen-rich reformat gas has drastic consequences on the electrical performances— $j(E)$  and  $P(E)$  curves—of a single proton-exchange membrane fuel cell [1].

On the other hand, the adsorption and electrooxidation of several alcohols (methanol, ethanol, etc.) in a direct-alcohol fuel cell (direct-methanol fuel cell [2, 3] or direct-ethanol fuel cell [4, 5]) involve the formation at a platinum electrode of adsorbed CO with different structures, such as linearly bonded CO ( $\text{CO}_L$ ), or bridge-bonded CO ( $\text{CO}_B$ ) [6], which acts as a strong poisoning species of the Pt-based catalysts used for the electrooxidation reaction. Thus, investigations of the interaction of CO with Pt electrodes presenting different surface structures (polycrystalline platinum, shape-controlled platinum nanoparticles exhibiting preferentially oriented nanosurfaces and real spherical fuel cell nanoparticles) and comparison with Pt(hkl) single crystals is of prime importance to elucidate the reaction mechanisms [7] and to improve the electrocatalytic activity. It can be mentioned that depending on the platinum catalyst surface structure [8], the CO oxidation reaction may lead to kinetic instabilities in the presence of other species such as hydrogen [8, 9] or inhibiting anions [10].

In this paper, we will present and discuss some results on CO adsorption and oxidation at several Pt electrocatalysts with different surface structures (single crystal surfaces, oriented nanosurfaces and real fuel cell nanoparticles) obtained by the combination of electrochemical methods and infrared reflectance spectroscopy (electrochemically modulated infrared reflectance spectroscopy (EMIRS) [11], subtractively normalized interfacial Fourier transform infrared reflection spectroscopy (SNIFTIRS) [12] and single potential alteration infrared reflection spectroscopy (SPAIRS) [13]). In particular, we will try to correlate the

peak multiplicity observed in the voltammograms of CO oxidation with the structure and morphology of the platinum electrocatalyst.

## Experimental

### Platinum Nanoparticle Synthesis and Characterization [14–16]

Platinum catalysts were prepared using previously described methods, which are relevant to obtain nanoparticles exhibiting clean surface for further electrochemical investigations [17]. Briefly, spherical Pt nanoparticles were synthesized by the *water-in-oil* microemulsion method (w/o method). A first microemulsion consisting in a *n*-heptane/Brij<sup>®</sup>30/water system ( $n_{\text{water}}/n_{\text{Brij}^{\text{®}}30}=3.8$ ) with 0.1 M  $\text{H}_2\text{PtCl}_6$ , 6  $\text{H}_2\text{O}$  (99.9%, Alfa Aesar) was mixed at 25 °C with a second one containing 1.5 M sodium borohydride, with  $n_{\text{water}}/n_{\text{Brij}^{\text{®}}30}=3.8$  and  $n_{\text{NaBH}_4}/n_{\text{Pt}}=15$ . This procedure is referred to as the Pt-w/o method.

Preferentially shaped Pt nanoparticles were prepared by the polyacrylate method (PA method). The PA method involved the reduction of  $\text{K}_2\text{PtCl}_4$  for nanocubes or  $\text{K}_2\text{PtCl}_6$  for the other shapes in an aqueous solution of sodium polyacrylate (PA, with a mean molecular mass of  $2,100 \text{ g mol}^{-1}$ ). The PA/Pt molar ratio and pH value of the reaction medium were varied in order to obtain either octahedral or cuboctahedral nanoparticles. To obtain cubic nanoparticle, the pH is fixed at 9.0 and PA/Pt=1; this procedure is referred to as the Pt-PA1 method. To obtain tetrahedral and octahedral nanoparticles, the pH was adjusted to 7.0 and PA/Pt=1; this procedure is referred to as the Pt-PA2 method. To obtain cuboctahedral nanoparticles, the pH was adjusted to 9.0 PA/Pt=5; this procedure is referred to as the Pt-PA3 method.

Characterizations by TEM (sizes and shapes) and by electrochemical methods (surface domains proportions by oxidation of spontaneous adsorbed Bi and Ge) [18, 19] are summarized in Table 1.

**Table 1** Estimation of the particle size and shape from TEM measurements and of the surface-ordered domain ratios by the bismuth and germanium adatom methods [18, 19]

	TEM		Electrochemical methods	
	Size/nm	shapes	% (100)	% (111)
Pt-w/o	3–5	Spheres	10	10
Pt-PA1	8–10	Cubes	42	18
Pt-PA2	10–12	Octahedrons/tetrahedrons	14	44
Pt-PA3	10–12	cuboctahedrons	26	36

### Rapid Scan Cyclic Voltammetry

The potential-time programme shown in Fig. 1 was used for adsorption measurements, with a scan rate  $\nu$  of  $10 \text{ V s}^{-1}$ . This scan rate is sufficiently low to allow the complete oxidation of adsorbed CO and sufficiently high to avoid any further adsorption of CO. Different adsorption times  $t_{\text{ads}}$  and different adsorption potentials  $E_{\text{ads}}$  were used. Before CO adsorption, the potential sweep was limited to an upper limit  $E'_a$ , low enough to prevent any surface reconstruction. After CO adsorption during the time  $t_{\text{ads}}$ , a single cycle was run with an upper limit  $E_a$  greater than  $E'_a$ ; and sufficiently high to oxidize completely the adsorbed CO layer.

### Infrared Reflectance Spectroscopy

The first “in situ” infrared reflectance spectroscopy under electrochemical control of the working electrode in a three-electrode cell was realized using the so-called EMIRS. Experimental details of this external reflection technique are fully described in textbooks [11]. Later on, due to the development of Fourier transform infrared reflectance spectroscopy (FTIRS), this last technique was adapted to the “in situ” observation of adsorbed species and reaction products at the electrode–electrolyte interface [12, 13]. Some important details of these techniques are described below.

The working electrode consisted of a mirror polished platinum disc or a gold disc or a glassy carbon (GC) disc (diameter 8 mm) glued to a glass tube as the holder. For nanoparticle powders, the catalyst suspension was deposited on the GC disc and the solvent was evaporated under a pure nitrogen stream.

With the SNIFTIRS technique [12], like in EMIRS, the working electrode potential is modulated between two values ( $E_i$  and  $E_f$ ) according to a square wave signal (frequency of potential modulation typically 0.025 Hz). The reflectivity was obtained at these two electrode potentials and resulted from the co-addition of 128 interferograms 30 times at each

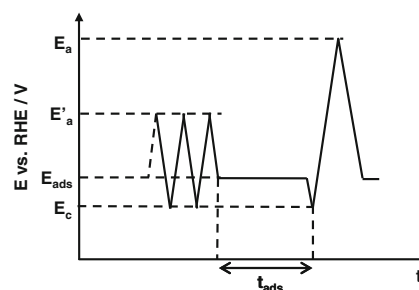


**Fig. 1** Potential-time programme used to oxidize CO adsorbed at a constant potential  $E_{\text{ads}}$  during time  $t_{\text{ads}}$ ; before CO adsorption, the positive limit  $E'_a$  is chosen to avoid any reconstruction of the electrode surface

potential. Final spectra were calculated as a differential reflectivity:

$$\left(\frac{\Delta R}{R}\right) = \left(\frac{R_{E_f} - R_{E_i}}{R_{E_i}}\right) \quad (1)$$

where  $R_{E_i}$  is the reflectivity at the initial potential  $E_i$  and  $R_{E_f}$  is the reflectivity at the final potential  $E_f$  of the square wave modulation with  $\Delta E = E_f - E_i = \text{constant}$ .

With the SPAIRS technique [13], the electrode reflectivity was recorded each 0.1 V during the first slow voltammetric scan at  $0.001 \text{ V s}^{-1}$ . Each spectrum resulted from the co-addition of 128 interferograms. The data acquisition required 20 s, i.e. over  $\approx 0.02 \text{ V}$ . Final spectra were normalized as a change  $\Delta A_n$  in absorbance:

$$\Delta A_n = \frac{\Delta A}{N} = -\frac{1}{N} \left(\frac{\Delta R}{R}\right) = -\frac{1}{N} \left(\frac{R_E - R_{E_{\text{ref}}}}{R_{E_{\text{ref}}}}\right) \quad (2)$$

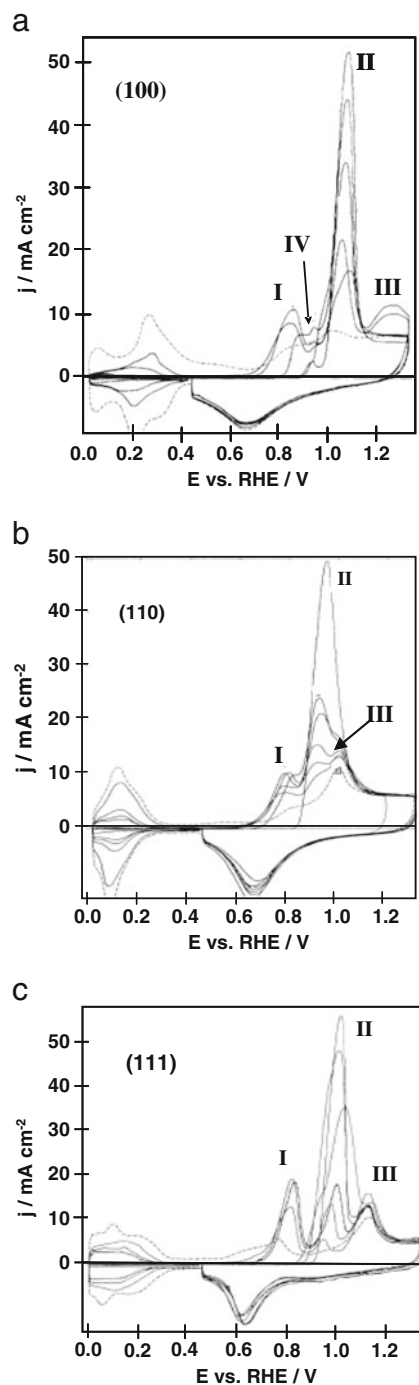
where  $N = (E - E_{\text{ref}})/(0.1 \text{ V})$ ,  $R_E$  is the reflectivity taken at potential  $E$  during the voltammetric scan,  $R_{E_{\text{ref}}}$  that recorded at the most negative potential  $E_{\text{ref}}$  before cycling, and  $N$  is a number without units.

In both cases, for  $E > E_{\text{ref}}$ , a negative peak means the production of species and a positive band indicates the consumption of species at the electrode surface.

## Results and Discussion

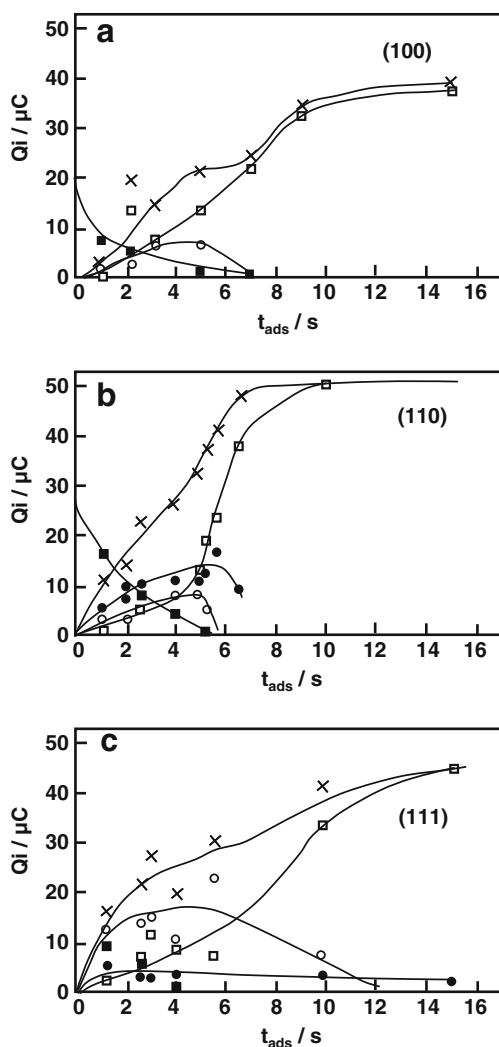
### Adsorption and Electrooxidation of CO at Pt(hkl) Single Crystals

Figure 2 shows the  $j(E)$  curves recorded according to the programme of Fig. 1 in a CO-saturated acid electrolyte after the adsorption of CO for different  $t_{\text{ads}}$  at  $E_{\text{ads}} = 0.45 \text{ V vs. RHE}$  for Pt (100), Pt (110) and Pt (111) surfaces, respectively. For  $t_{\text{ads}} < 5 \text{ s}$ , the  $j(E)$  curves show at least three anodic current peaks labelled I, II and III, respectively. However for the Pt (100) plane, a small oxidation peak, labelled IV, may also be observed, and peak III is not always displayed. Peaks I and II are presumably related to the direct oxidation of adsorbed CO, whereas peak III, which occurs at higher potentials, where the electrode surface is usually oxidized, may result from the indirect oxidation of bulk CO by surface oxides, as already observed on polycrystalline platinum [20]. As the adsorption time  $t_{\text{ads}}$  increases, the quantity of electricity related to the oxidation of adsorbed hydrogen decreases and that related to the oxidation of adsorbed CO increases. For  $t_{\text{ads}} > 6 \text{ s}$ , the anodic  $j(E)$  profile is characterized by the disappearance of peak I and an increase of the intensity of peak II [21], for the three orientations. The quantities of electricity under each peak obtained for the CO oxidation were determined by subtracting the cyclic



**Fig. 2** Voltammograms of a Pt (100) single crystal plane electrode (a); Pt (110) single crystal plane electrode (b); Pt (111) single crystal plane electrode (c); in a CO-saturated solution ( $0.5 \text{ M HClO}_4$ ,  $25 \text{ }^\circ\text{C}$ ,  $10 \text{ V s}^{-1}$ ,  $E_{\text{ads}} = 0.45 \text{ V vs. RHE}$ ) for various adsorption times (in the range 1.1 to 30 s). (dash line) Blank electrolyte

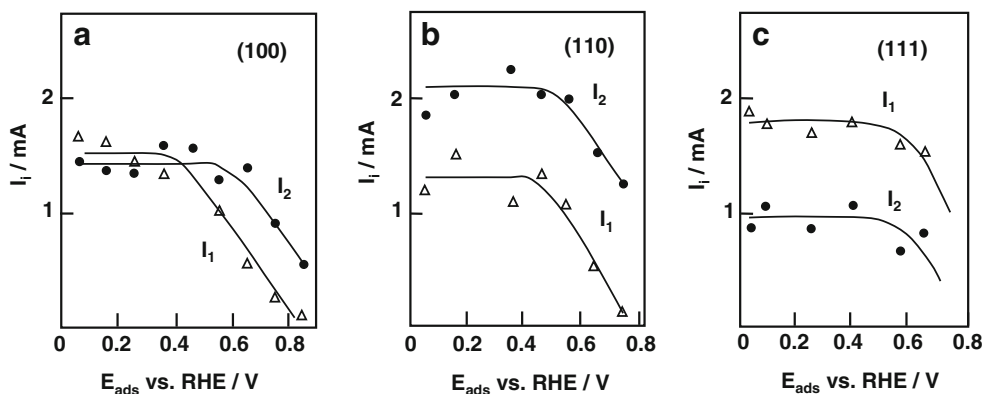
voltammograms recorded under the same conditions in  $\text{N}_2$ -saturated supporting electrolyte. Figure 3 gives the charge involved in each peak  $Q_i$ , the total charge due to CO electrooxidation ( $Q_{\text{total}}$ ) and that related to H adsorption ( $Q_{\text{H}}$ ) as a function of  $t_{\text{ads}}$  for the three planes. The charge associated with



**Fig. 3** Plots vs.  $t_{\text{ads}}$  of the quantity of electricity  $Q_i$  associated with the oxidation of the different CO species adsorbed at  $E_{\text{ads}}=0.45$  V vs. RHE. (Blank circle)  $Q_1$ ; (blank square)  $Q_2$ ; (filled circle)  $Q_3$ ; (cross) the total of adsorbed CO ( $Q_{\text{total}}$ ); (filled square) adsorbed hydrogen ( $Q_{\text{H}}$ ). **a** Pt (100); **b** Pt(110); **c** Pt(111)

peak I ( $Q_1$ ) always presents a maximum for  $t_{\text{ads}} \sim 5$  s, and that related to peak II ( $Q_2$ ) has the same qualitative shape for the three planes. The charge related to the H adatom

**Fig. 4** Plots of the peak current intensities  $I_i$  recorded during the oxidation of adsorbed CO as a function of the adsorption potential  $E_{\text{ads}}$  (0.5 M HClO<sub>4</sub>, 25 °C, 10 V s<sup>-1</sup>).  $I_1$  corresponds to peak I and  $I_2$  to peak II. **(a)** Pt (100),  $t_{\text{ads}}=3$  s; **(b)** Pt (110),  $t_{\text{ads}}=4.2$  s; **(c)** Pt (111),  $t_{\text{ads}}=3$  s



electrosorption process decreases with increasing  $t_{\text{ads}}$ , reaching 0 for  $t_{\text{ads}} \sim 6$  s. In good agreement with previous results on fully covered polycrystalline platinum [20, 22], two electrons are required at one Pt site of each plane for the oxidation of the kind of CO molecule (linearly bonded CO) which prevails at high coverage as the limiting value obtained for  $Q_2$  and for  $Q_{\text{total}}$  is twice that measured for  $Q_{\text{H}}$  at  $t_{\text{ads}} \sim 0$ .

However, some differences between the three planes are evidenced. On the (110) plane the increase of the  $Q_2$  value after about 5 s is very sharp and occurs in a very narrow range of adsorption time (ca. 5.5 s). The origin of peak III is difficult to assign, particularly for Pt (100). However, for Pt (110) and Pt (111), this peak seems to be connected with the oxygen adsorption process, which occurs simultaneously with the electrooxidation of CO.

Figure 4 reports the behaviour of the current peaks I and II associated with the oxidation of adsorbed CO obtained at constant  $t_{\text{ads}}$  and different  $E_{\text{ads}}$ . For the three planes, the intensity of both peaks remain constant for CO adsorption potential ranges where adsorbed hydrogen exists and where oxidation of the surface does not occur ( $E_{\text{ads}} < 0.4$  to 0.6 V vs. RHE, depending on the single crystal plane). This indicates that there is no net interaction between  $\text{CO}_{\text{ads}}$  and  $\text{H}_{\text{ads}}$ . The adsorption potential sequence for which the decrease of the current peak I intensity starts is in agreement with that for the oxygen adsorption in blank electrolyte (Pt (100) < Pt (110) < Pt (111) [23]), indicating that the decreases of peak I intensity is the consequence of competitive adsorption of CO and OH, leading to CO oxidation.

#### Infrared Reflectance Spectroscopic Investigations of CO Adsorption at Smooth Pt-Based Electrodes

##### EMIRS Studies of CO Adsorption

In order to explain the multiplicity of CO oxidation peaks observed on single crystal platinum electrodes by a model involving the participation of different CO adsorbed states, Beden et al. [24] investigated by EMIRS the adsorbed CO species resulting from methanol chemisorption on the three

low index single crystal platinum surfaces: Pt(100), Pt(110) and Pt(111). Figure 5 displays the EMIRS spectra of the adsorbed CO species resulting from methanol adsorption recorded at a mean electrode potential of 0.35 V vs. RHE. At Pt(100), a large contribution of the species responsible of the band at 1,680–1,700  $\text{cm}^{-1}$  is observable. This band was assigned to multibonded CO ( $\text{CO}_m$ ) adsorbed on platinum. The band at 1,870  $\text{cm}^{-1}$  was assigned to bridge-bonded CO ( $\text{CO}_B$ ). Both these absorption bands are positive, which indicates that the corresponding electroadsorbates have been formed at the lower potential limit. The last band, centred at 2,050  $\text{cm}^{-1}$ , asymmetric, was attributed to linearly bonded  $\text{CO}_L$ . This asymmetry indicated that the  $\text{CO}_L$  contribution is higher at the higher potential limit.

The adsorption of CO on a smooth polycrystalline Pt electrode also displays several adsorbed states as shown in Fig. 6. The spectrum was obtained over the range from 1,750 to 2,350  $\text{cm}^{-1}$  by modulating the electrode potential between 0 and 0.35 V vs. RHE with a square wave at 8.5 Hz. A strong bipolar band centred at 2,090  $\text{cm}^{-1}$  and a very weak band, which might also be bipolar, near 1,860  $\text{cm}^{-1}$  can be seen. The potential dependence of the absorption spectrum was recorded at fixed modulation amplitude (Fig. 7). The CO band intensity decreases only slowly when increasing the electrode potential and the band completely disappeared at potentials greater than 0.8 V, with the appearance of a new band at around 2,350  $\text{cm}^{-1}$ .

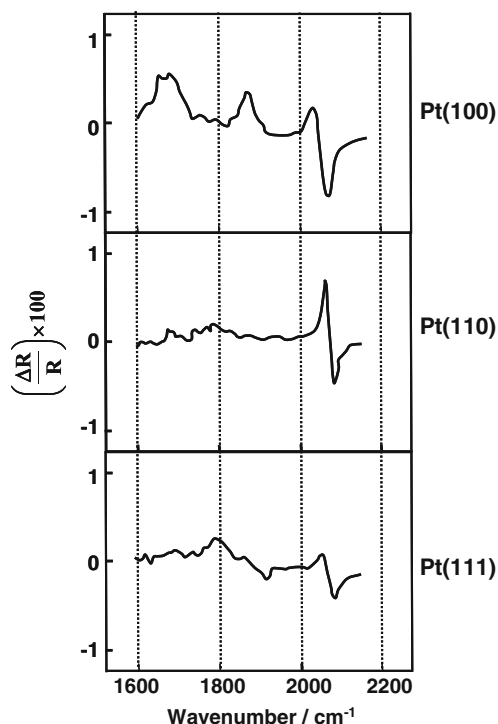


**Fig. 5** EMIRS spectra of adsorbed CO species resulting from methanol adsorption in 0.1 M  $\text{HClO}_4$ +0.5 M  $\text{CH}_3\text{OH}$  at a Pt single crystal electrode;  $E=0.35$  V vs. RHE,  $\Delta E=0.35$  V,  $f=13.6$  Hz

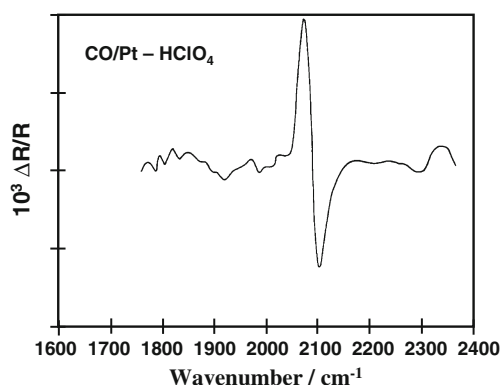


**Fig. 6** Reflectance spectrum from polycrystalline Pt in 1 M  $\text{HClO}_4$ , CO-saturated solution. Modulation from 0 to 0.350 V vs. RHE at 8.5 Hz. Scan rate 0.0127  $\mu\text{m s}^{-1}$

Moreover, the position of the main absorption band at 2,090  $\text{cm}^{-1}$  (assigned to linearly bonded CO) shifts to lower values as the electrode potential is made more positive. The observed shift is a combination of two factors [25]: a shift to higher energy with increasing positive potential and a shift to lower energy with decreasing the amount of adsorbed species. The first effect is due to changes in the extent of back bonding from the metal to the  $\pi^*$  antibonding orbital of the  $\text{CO}_{\text{ad}}$  as the effective electronegativity of the metal is varied and, of course, it is this effect which causes the basic bipolar shape of the bands. The second effect is dominantly produced by interactions among the neighbouring dipole oscillators. In the present case, depletion effects which cause a lowering of surface coverage at the higher positive potentials lead to a net shift to lower energy. It should be noted that the oxidation process at 0.8 V which leads to the consumption of adsorbed CO and, consequently, to the disappearance of the corresponding absorption bands, also blocks the surface towards further CO adsorption when the electrode potential is lowered; to re-adsorb CO, it was found necessary to take the potential right down into the hydrogen region for several minutes. This “irreversible” process indicates the existence of strongly bonded species, but might also be related to changes occurring in the oxide layer as a

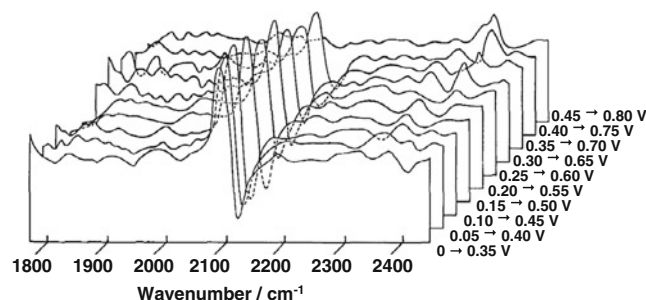


**Fig. 7** Reflectance spectrum at various potentials and a constant modulation amplitude of 0.35 V, for polycrystalline Pt in 1 M  $\text{HClO}_4$ , CO-saturated solutions, at 25 °C. Modulation at 8.5 Hz



result of the square wave modulation of the electrode potential. On the other hand, the band clearly observed at around  $2,350\text{ cm}^{-1}$  could be attributed to  $\text{CO}_2$ ; it is interesting to follow its evolution as a function of the anodic limit of the pulse and to note that it already appears at potentials as low as  $0.35\text{ V}$  vs. RHE.

#### FTIR Study of CO Oxidation at Smooth Pt Electrodes

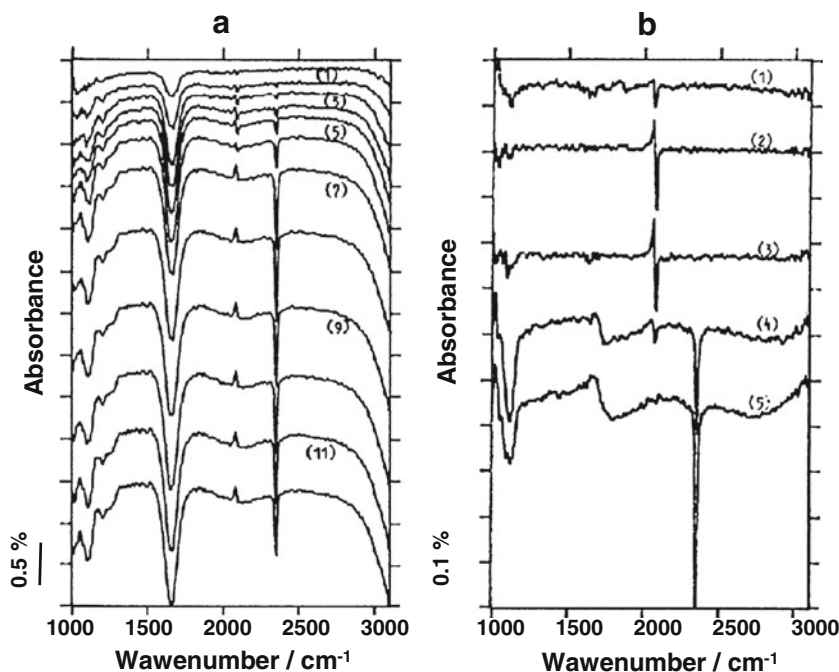
The CO oxidation reaction was examined using infrared reflectance spectroscopy in a CO-saturated  $0.5\text{ M}$  perchloric acid solution [26]. After CO adsorption at  $0.07\text{ V}$ , the electrode potential was swept positively (at  $0.001\text{ Vs}^{-1}$ ) until  $0.77\text{ V}$  and the SPAIR spectra at a smooth Pt electrode were recorded at potential intervals of  $0.05\text{ V}$  with a reference spectrum taken at  $0.07\text{ V}$  (Fig. 8a). The band observed at  $2,050\text{ cm}^{-1}$  at low electrode potentials corresponds to linearly adsorbed CO. Its intensity increased between  $0.12$  and  $0.32\text{ V}$  and then decreased for potentials greater than  $0.37\text{ V}$ . The band assigned to the formation of  $\text{CO}_2$  is observed at  $2,350\text{ cm}^{-1}$  for potentials greater than  $0.17\text{ V}$ . No other significant band is observed in this spectrum, except those assigned to perchlorate ions ( $1,100\text{ cm}^{-1}$ ) and interfacial water ( $1,600\text{ cm}^{-1}$ ). Similarly, the SNIFTIR spectra, recorded at a smooth Pt electrode at low potentials, display a bipolar band at  $2,050\text{ cm}^{-1}$  assigned to linearly bonded  $\text{CO}_L$  (Fig. 8b). Its intensity increased with the electrode potential from  $0.22$  to  $0.42\text{ V}$ . At  $0.52\text{ V}$ , the  $\text{CO}_L$  band intensity decreased and the band corresponding to adsorbed  $\text{CO}_2$  appeared. The  $\text{CO}_L$  was completely oxidized at  $0.62\text{ V}$ .

#### CO Oxidation on Platinum Nanoparticles

The oxidation of a chemisorbed saturated layer of CO on platinum nanoparticles gives rise to a multiplicity of oxidation peaks over a wide potential range from ca.  $0.35$  to  $0.8\text{ V}$ , as shown in Fig. 9 in the case of nanocuboctedrons/truncated nanooctaedrons obtained from the Pt-PA3 method, as an example.

On Pt-nanocubes synthesized according to the Pt-PA1 method, Brimaud et al. recorded voltammograms of the oxidation of a saturating CO layer at different potential scan rates [14]. They observed a shift of the oxidation peaks towards higher potentials as the scan rate  $\nu$  was increased. The  $dE/d(\log \nu)$  values of  $0.080$  and  $0.064\text{ V decade}^{-1}$  were determined for peaks A and B (Fig. 10), respectively. These results were compared with experiments carried out on single crystals with low Miller indices: Palakis et al. [27] found  $0.080\pm 0.005$  and  $0.060\pm 0.003\text{ V decade}^{-1}$  for Pt (111) and Pt(100) surfaces, respectively; whereas Lai et al. [28] determined  $0.075\pm 0.003$  and  $0.081\pm 0.003\text{ V decade}^{-1}$  for Pt(111) and Pt(110) surfaces, respectively. Peak B at high potentials displayed the same behaviour as for the oxidation of  $\text{CO}_{\text{ads}}$  on a (100) surface, whereas peak A contained the contribution of  $\text{CO}_{\text{ads}}$  oxidation on (111) surface and on low coordination sites. In a recent paper [16], a detailed analysis of the CO stripping oxidation peaks have indeed revealed the presence of up to four voltammetric features: a pre-peak involving nanometric surface domains, and three peaks assigned to the presence of surface domains which are either preferentially oriented or disordered. Peak A was decomposed into two contributions, one

**Fig. 8** **a** SPAIR spectra at a smooth Pt electrode recorded in a CO saturated  $0.5\text{ M HClO}_4$  solution,  $E_{\text{ads}}=0.070\text{ V}$  vs. RHE, reference spectrum taken at  $0.070\text{ V}$  vs. RHE, scan rate  $0.001\text{ Vs}^{-1}$ . Electrode potentials in volts vs. RHE: (1)  $0.12$ , (2)  $0.17$ , (3)  $0.22$ , (4)  $0.27$ , (5)  $0.32$ , (6)  $0.37$ , (7)  $0.42$ , (8)  $0.47$ , (9)  $0.52$ , (10)  $0.57$ , (11)  $0.62$ , (12)  $0.67$ . **b** SNIFTIR spectra of CO adsorption and oxidation at a smooth platinum electrode in  $0.5\text{ M HClO}_4$ , potential windows in volts vs. RHE: (1)  $0.07\text{--}0.37$ , (2)  $0.17\text{--}0.47$ , (3)  $0.27\text{--}0.57$ , (4)  $0.37\text{--}0.67$ , (5)  $0.47\text{--}0.77$



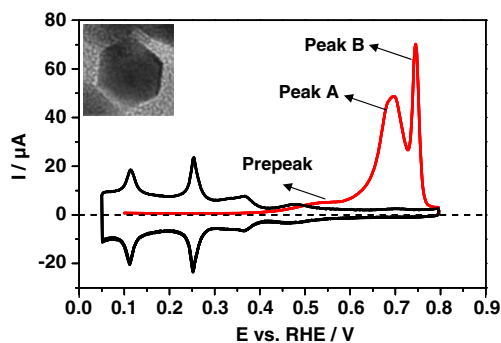


**Fig. 9** Voltammograms obtained for Pt cubooctahedral nanoparticles:  $\text{CO}_{\text{ads}}$  oxidative stripping voltammograms (red lines) and subsequent cyclic voltammograms (black lines) in CO-free electrolyte;  $E_{\text{ads}}=0.1$  V vs. RHE, scan rate  $0.02 \text{ V s}^{-1}$ . The transmission electron microscopy images are given in the inset

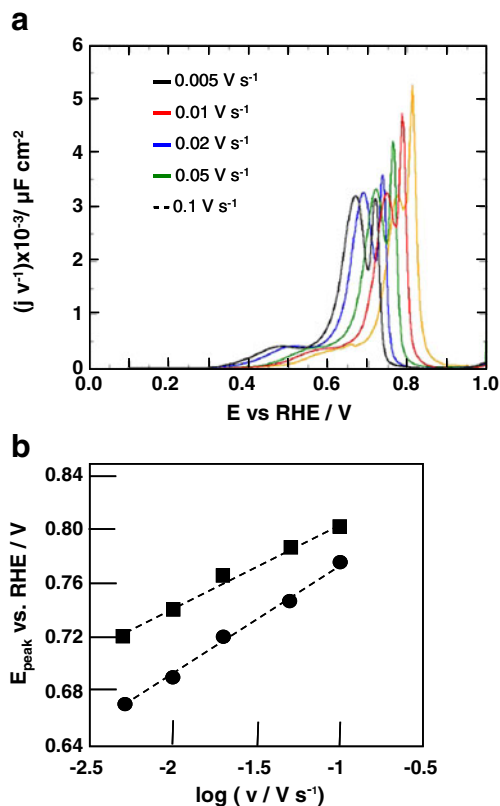
at lower potentials due to oxidation of CO adsorbed on (111) surface domains, the other one at higher potentials involves the low coordinated sites and the surface defects, and peak B was assigned to oxidation of  $\text{CO}_{\text{ads}}$  on (100) surface domains. In Fig. 10, when the potential scan rate,  $\nu$ , increases from  $0.005$  to  $0.1 \text{ V s}^{-1}$  the oxidation onset potential shifts from ca.  $0.3$  to ca.  $0.4$  V vs. RHE and peaks A and B shift towards higher potentials; however, since the shift of peak A with the scan rate is higher than that of peak B, peak A becomes a shoulder of peak B at high potential scan rates. The faradic charges associated with the pre-peak and with peak A are not affected by the potential scan rate. So, no faradic charge transfer from peak B or from the pre-peak towards peak A has been detected.

In order to complete these studies, measurements were also carried out in a CO-saturated electrolyte. Figure 11a, b, c show the  $j(E)$  curves recorded according to the programme of Fig. 1 in a CO-saturated acid electrolyte after the adsorption of CO for different  $t_{\text{ads}}$  at  $E_{\text{ads}}=0.45$  V vs. RHE for Pt-PA1 (nanocubes), Pt-PA2 (tetrahedrons/octahedrons) and Pt-PA3 (cubooctahedrons), as well as the related CO stripping voltammograms recorded at  $0.1 \text{ V s}^{-1}$ . The scan rate was limited to  $0.1 \text{ V s}^{-1}$  since for higher scan rates, the CO oxidation peaks were shifted towards too high potentials, which was detrimental for the fragile nanoparticle surface structure, leading to strong surface reconstruction [14, 29]. The  $j(E)$  curves recorded in a CO-saturated medium showed four anodic current peaks labelled I, II, III and IV. At first, peak I increases with increasing the CO surface coverage, and then decreases for high CO surface coverage. Peak II and III increased with increasing the CO surface coverage. These peaks likely correspond to peaks A and B observed at lower potentials in the CO stripping voltammograms, but shifted towards higher potentials, since they display similar general behaviour. Peak IV is certainly due to oxidation of CO on Pt oxidized surface, as described previously on Pt single crystal surfaces with low Miller indices, since it

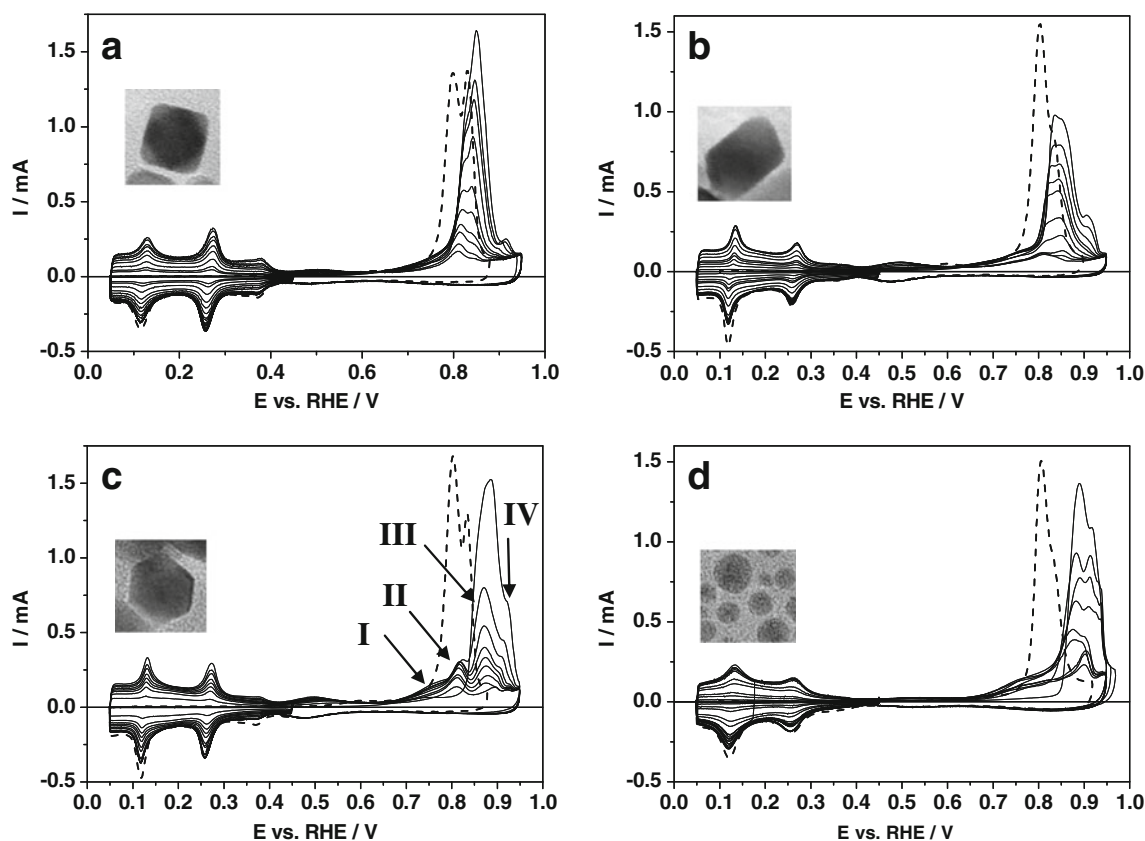
appears in a potential region where the Pt surface starts to be oxidized.

Figure 11d displays the CO oxidation voltammograms recorded on nanoparticles prepared by the water-in-oil microemulsion method [14, 16, 17]. Such nanoparticles are spherical, display a mean size of ca.  $3 \text{ nm}$  and are very similar to those used as fuel cell electrode catalysts once supported on a carbon powder substrate [30]. The general shapes of the CVs are the same as for the preferentially oriented nanoparticles, exhibiting three peaks. However, peak I appears much more pronounced. This peak was not discussed in the previous part concerning the CO oxidation on platinum-oriented nanosurface crystals. A first explanation to the presence of this peak could be a correspondence with the pre-peak which is observed on stepped surface [31, 32] or shaped nanoparticles [14, 16, 17]. But, on spherical nanoparticles the pre-peak is very small or inexistent, as shown in Fig. 11d. Moreover, such pre-peak appears at very high surface coverage, after CO adsorption at potentials lower than  $0.3$  V vs. RHE [33]. Therefore, this first explanation has to be discarded.

The peak multiplicity could be explained by the nature of adsorbed CO. Sato et al. [34] carried out electrochemical ATR-FTIRAS measurements (Attenuated Total Reflection–



**Fig. 10** a  $\text{CO}_{\text{ads}}$  oxidative stripping curves recorded at different potential scan rates on nanocube particles (Pt-PA1 method); scan rates  $\nu=0.005, 0.01, 0.02, 0.05$  and  $0.1 \text{ V s}^{-1}$ . b  $E_{\text{peak}}=f(\ln \nu)$  straight lines: (filled circle) peak A, (filled square) peak B ( $T=25$  °C,  $0.5 \text{ M H}_2\text{SO}_4$ )



**Fig. 11** Voltammograms obtained for Pt nanoparticles of various shapes: **a** cubic from Pt-PA1 method, **b** octahedral from Pt-PA2 method, **c** cuboctahedral from Pt-PA3 method and **d** spherical from w/o method recorded in a CO-saturated solution (0.5 M H<sub>2</sub>SO<sub>4</sub>, 25 °C,

0.1 V s<sup>-1</sup>,  $E_{\text{ads}}=0.45$  V vs. RHE) for various adsorption times (i.e. for various CO coverages). (Dash line) Corresponding CO stripping curves at 0.1 V s<sup>-1</sup> ( $E_{\text{ads}}=0.1$  V vs. RHE)

Fourier Transform Infrared Reflectance Absorption spectroscopy) to investigate the nature of CO adsorbed under potential control (0.05 V vs. RHE) on a highly dispersed Pt catalyst with an average particle size of 2.6 nm supported on carbon black (Pt/C). The CO content was fixed to 1 and 100 % CO atmospheres, leading to CO coverage  $\theta_{\text{CO}}$  of 0.69 and 1, respectively. They recorded two well-defined  $\nu(\text{CO})$  bands assigned to CO<sub>L</sub> and bridge-bonded CO<sub>B</sub> (symmetric mode). From their results, they proposed a simultaneous occupation of terrace (CO<sub>L</sub> terrace) and step-edge sites (CO<sub>L</sub> edge). They also observed a new band located close to 1,950 cm<sup>-1</sup>, which was assigned to asymmetric bridge-bonded CO<sub>B(asym)</sub> adsorbed on (100) terraces. The frequency  $\nu(\text{CO})$  of CO<sub>L</sub> appeared, at a given potential, lower by 30–40 cm<sup>-1</sup> than that recorded at a Pt poly- or single crystals, which was interpreted as a stronger Pt–CO electronic interaction in the case of the nanoparticles, and/or a higher contribution of defects (steps and edges).

Another explanation can be given, by correlating the CO stripping voltammograms recorded on defined shape-oriented Pt nanoparticle surfaces with the CO oxidation recorded on Pt nanoparticles: while some Pt sites become free of CO, OH adsorption takes place and the oxidation of

CO on larger (111) and (100) surface domains can occur, giving rise to peaks II and III. However, the competition between OH and CO adsorption on the free Pt sites leads to a delay in the oxidation of CO adsorbed on larger (100) and (111) surface domains.

## Conclusion

The study of CO/Pt surface interaction is of paramount importance in the field of electric energy production with low-temperature fuel cell systems. However, although CO is a small molecule, its oxidation mechanism on a Pt surface involving only the exchange of two electrons is very complex and leads to a multiplicity of oxidation peaks from ca. 0.35 V to ca. 1.0 V vs. RHE, i.e. a difference in free energy of ca. 125 kJ mol<sup>-1</sup>. This significant change in  $\Delta_r G^0$  is either explained in terms of exhibited surface domains and sites on single crystals with low Miller indices [24], stepped surfaces [35–37] and shaped nanoparticles [14, 16, 38], or of size effect [39], or of agglomeration effect [40], and or of the structure of chemisorbed CO (linear or multibonded) [21]. However, it seems that the main adsorbed CO species



at high adsorption times (high adsorption coverages) is the linearly bonded one, independent of the crystallographic structure although some bridged or multibonded species were also detected. Therefore, although the relationship between data obtained from single crystals with low Miller indices and vicinal surfaces, and nanoparticles is not completely achieved due to the high structure sensitivity of the CO oxidation reaction and needs further investigations, we proposed that the CO oxidation peak multiplicity on platinum is due to the presence of specific surface domains on Pt electrocatalysts, including a surface domain size effect.

## References

1. S.J. Lee, S. Mukerjee, E.A. Ticianelli, J. McBreen, *Electrochim Acta* **44**, 3283 (1999)
2. C. Lamy, J.M. Léger, S. Srinivasan, Direct methanol fuel cells: from a twentieth century electrochemist's dream to a twenty-first century emerging technology, in *Modern aspects of electrochemistry*, vol. 34, ed. by J.O'M. Bockris, B.E. Conway, R.E. White (Kluwer Academic/Plenum Publishers, New York, 2001), p. 53
3. A. Hamnett, Direct methanol fuel cells (DMFC), in *Handbook of fuel cells: fundamentals and survey of systems*, vol. 1, ed. by W. Vielstich, A. Lamm, H. Gasteiger (Wiley, Chichester, 2003), p. 305
4. C. Lamy, E.M. Belgsir, Other direct alcohol fuel cells, in *Handbook of fuel cells: fundamentals and survey of systems*, vol. 1, ed. by W. Vielstich, A. Lamm, H. Gasteiger (Wiley, Chichester, 2003), p. 323
5. C. Lamy, C. Coutanceau, J.M. Léger, The direct ethanol fuel cell: a challenge to convert bioethanol cleanly into electric energy, in *Catalysis for sustainable energy production*, ed. by P. Barbaro, C. Bianchini (Wiley-VCH, Weinheim, 2009), p. 3
6. B. Beden, A. Bewick, C. Lamy, K. Kunimatsu, *J Electroanal Chem* **121**, 343 (1981)
7. R. Adžič, Reaction kinetics and mechanisms on metal single-crystal electrode surfaces, in *Modern aspects of electrochemistry*, Vol. 21, ed. by E.W. White, J.O'M. Bockris, B.E. Conway (Plenum press, New York, 1990), p. 163
8. R.C. Yeates, J.E. Turner, A.J. Gellman, G.A. Somorjai, *Surf Sci* **149**, 175 (1985)
9. M.C. Deibert, D.L. Williams, *J Electrochem Soc* **116**, 1290 (1969)
10. S. Malkhandi, A. Bonnefont, K. Krischer, *Electrochem Comm* **7**, 710 (2005)
11. B. Beden, C. Lamy, Infrared reflectance spectroscopy, in *Spectroelectrochemistry—theory and practice*, ed. by R.J. Gale (Plenum Press, New York, 1988), p. 189
12. A. Bewick, B.S. Pons, Infrared spectroscopy of the electrode-electrolyte solution interface, in *Advances in infrared and Raman spectroscopy*, Vol. 12, ed. by R.J.H. Clark, R.E. Hester (Wiley et Sons, London, 1985), p. XI
13. D.S. Corrigan, M.J. Weaver, *J Electroanal Chem* **241**, 143 (1988)
14. S. Brimaud, S. Pronier, C. Coutanceau, J.M. Léger, *Electrochem Comm* **10**, 1703 (2008)
15. P. Urchaga, S. Baranton, T. Napporn, C. Coutanceau, *Electrocatalysis* **1**, 3 (2010)
16. P. Urchaga, S. Baranton, C. Coutanceau, G. Jierkiewicz, *Langmuir* **28**, 3658 (2012)
17. C. Coutanceau, P. Urchaga, S. Brimaud, S. Baranton, *Electrocatalysis* (2011). doi:10.1007/s12678-012-0079-0
18. J. Solla-Gullón, F.J. Vidal-Iglesias, P. Rodríguez, E. Herrero, J.M. Feliu, J. Clavilier, A. Aldaz, *J Phys Chem B* **108**, 13573 (2004)
19. J. Solla-Gullón, P. Rodríguez, E. Herrero, A. Aldaz, J.M. Feliu, *Phys Chem Chem Phys* **10**, 1359 (2008)
20. S. Bilmes, N. De Tacconi, A.J. Arvia, *J Electroanal Chem* **164**, 129 (1984)
21. B. Beden, S. Bilmes, C. Lamy, J.M. Léger, *J Electroanal Chem* **149**, 295 (1983)
22. M.W. Breiter, *J Electroanal Chem* **127**, 157 (1981)
23. K. Yamamoto, D.M. Kolb, R. Katz, G.V. Lempfuhr, *J Electroanal Chem* **96**, 233 (1979)
24. B. Beden, C. Lamy, N.R. de Tacconi, A.J. Arvia, *Electrochim Acta* **35**, 691 (1990)
25. A. Bewick, M. Razaq, J.W. Russell, *J Electroanal Chem* **256**, 165 (1988)
26. A. Kabbabi, R. Faure, R. Durand, B. Beden, F. Hahn, J.-M. Leger, C. Lamy, *J Electroanal Chem* **44**, 41 (1998)
27. L. Palaikis, D. Zurawski, M. Hourani, A. Wieckowski, *Surf Sci* **199**, 183 (1988)
28. S.C.S. Lai, N.P. Lebedeva, T.H.M. Housmans, M.T.M. Koper, *Topics Catal* **46**, 320 (2007)
29. S. Brimaud, *Caractérisation des propriétés physiques et électrochimiques de nanoparticules de platine*, PhD thesis (University of Poitiers, France, 2002)
30. C. Coutanceau, S. Baranton, T. Napporn (2011) Platinum Fuel cell nanoparticle syntheses: effect on morphology, structure and electrocatalytic behavior, in *Nanoparticles/Book 2*, Intech Open Access Publisher (ed.), Rijeka (Croatia). ISBN 979-953-307-859-4.
31. N. Lebedeva, *Role of crystalline defects in electrocatalysis*, Ph.D. thesis (University of Eindhoven, The Netherlands, 2002)
32. A. López-Cudero, A. Cuesta, C. Gutiérrez, *J Electroanal Chem* **579**, 1 (2005)
33. A. Cuesta, A. Couto, A. Rincón, M.C. Pérez, A. López-Cudero, C. Gutiérrez, *J Electroanal Chem* **586**, 184 (2006)
34. T. Sato, K. Kunimatsu, H. Uchida, M. Watanabe, *Electrochim Acta* **53**, 1265 (2007)
35. N.P. Lebedeva, M.T.M. Koper, E. Herrero, J.M. Feliu, R.A. van Santen, *J Electroanal Chem* **487**, 37 (2000)
36. N.P. Lebedeva, A. Rodes, J. Feliu, M.T.M. Koper, R.A. van Santen, *J Phys Chem B* **106**, 9863 (2002)
37. F.J. Vidal-Iglesias, J. Solla-Gullón, J.M. Campiña, E. Herrero, A. Aldaz, J.M. Feliu, *Electrochim Acta* **54**, 4459 (2009)
38. J. Solla-Gullón, F.J. Vidal-Iglesias, E. Herrero, J.M. Feliu, A. Aldaz, *Electrochem Comm* **8**, 189 (2006)
39. F. Maillard, M. Eikerling, O.V. Cherstiouk, S. Schreier, E. Savinova, U. Stimming, *Faraday Discuss* **125**, 357 (2004)
40. F. Maillard, E.R. Savinova, U. Stimming, *J Electroanal Chem* **599**, 221 (2007)